



HAL
open science

Reverse-Bias Current Hysteresis at Low Temperature in GaN Schottky Barrier Diodes

B. Orfao, Mahmoud Abou Daher, R. A. Peña, B. G. Vasallo, S. Pérez, I. Íñiguez-De-La-Torre, G. Paz-Martinez, J. Mateos, Y. Roelens, M. Zaknounge, et al.

► **To cite this version:**

B. Orfao, Mahmoud Abou Daher, R. A. Peña, B. G. Vasallo, S. Pérez, et al.. Reverse-Bias Current Hysteresis at Low Temperature in GaN Schottky Barrier Diodes. *Journal of Applied Physics*, 2024, 135 (1), pp.014501. 10.1063/5.0177853 . hal-04405976

HAL Id: hal-04405976

<https://hal.science/hal-04405976v1>

Submitted on 25 Nov 2024

HAL is a multi-disciplinary open access archive for the deposit and dissemination of scientific research documents, whether they are published or not. The documents may come from teaching and research institutions in France or abroad, or from public or private research centers.

L'archive ouverte pluridisciplinaire **HAL**, est destinée au dépôt et à la diffusion de documents scientifiques de niveau recherche, publiés ou non, émanant des établissements d'enseignement et de recherche français ou étrangers, des laboratoires publics ou privés.














Distributed under a Creative Commons Attribution - NonCommercial 4.0 International License

RESEARCH ARTICLE | JANUARY 05 2024

Reverse-bias current hysteresis at low temperature in GaN Schottky barrier diodes

Special Collection: [Native Defects, Impurities and the Electronic Structure of Compound Semiconductors: A Tribute to Dr. Wladyslaw Walukiewicz](#)

B. Orfao ; M. Abou Daher ; R. A. Peña ; B. G. Vasallo ; S. Pérez ; I. Íñiguez-de-la-Torre ; G. Paz-Martínez ; J. Mateos ; Y. Roelens ; M. Zaknourne ; T. González 



J. Appl. Phys. 135, 014501 (2024)

<https://doi.org/10.1063/5.0177853>



Articles You May Be Interested In

Comprehensive model for ideal reverse leakage current components in Schottky barrier diodes tested in GaN-on-SiC samples

J. Appl. Phys. (July 2022)



Journal of Applied Physics

Special Topics Open for Submissions

[Learn More](#)

Reverse-bias current hysteresis at low temperature in GaN Schottky barrier diodes

Cite as: J. Appl. Phys. 135, 014501 (2024); doi: 10.1063/5.0177853

Submitted: 25 September 2023 · Accepted: 17 December 2023 ·

Published Online: 5 January 2024



B. Orfao,^{1,2,a)} M. Abou Daher,² R. A. Peña,¹ B. G. Vasallo,¹ S. Pérez,¹ I. Íñiguez-de-la-Torre,¹
G. Paz-Martínez,¹ J. Mateos,¹ Y. Roelens,² M. Zaknourne,² and T. González¹

AFFILIATIONS

¹Dpto. Física Aplicada and USAL-NANOLAB, Universidad de Salamanca, 37008 Salamanca, Spain

²CNRS-IEMN, Université de Lille, UMR8520, Av. Poincaré, 59650 Villeneuve d'Ascq, France

Note: This paper is part of the Special Topic on Native Defects, Impurities and the Electronic Structure of Compound Semiconductors: A Tribute to Dr. Wladyslaw Walukiewicz.

^{a)} **Author to whom correspondence should be addressed:** beatrizorfao@usal.es

ABSTRACT

In this paper, we report an analysis of reverse current mechanisms observed in GaN Schottky barrier diodes leading to hysteretic behavior of the I–V curves at low temperature. By means of DC measurements from 33 to 475 K, we demonstrate the presence of two leakage mechanisms when comparing the experiments with the results obtained using a unified model to predict the ideal reverse current of the diode. Poole–Frenkel emission is the dominant mechanism for temperatures above 200 K, while trap-assisted tunneling prevails for lower temperatures, where also, hysteresis cycles are revealed by means of DC dual-sweep voltage measurements. The energy of the corresponding traps has also been determined, being around 0.2 and 0.45 eV, respectively. The hysteresis phenomenon is attributed to the bias-induced occupancy of the energy states originating the leakage-current processes, which leads to the reduction of the reverse current after a high negative voltage is applied to the diode.

© 2024 Author(s). All article content, except where otherwise noted, is licensed under a Creative Commons Attribution-NonCommercial 4.0 International (CC BY-NC) license (<https://creativecommons.org/licenses/by-nc/4.0/>). <https://doi.org/10.1063/5.0177853>

I. INTRODUCTION

Terahertz technology has advanced significantly during the last few decades; however, there are still challenges, such as the development of solid-state THz devices capable of generating signals with an appropriate power level in this frequency range.¹ Schottky barrier diodes (SBDs) play an important role in solid-state THz sources based on frequency multiplication, with GaAs being the dominant technology. GaAs SBDs are used in multiple applications due to its good performance as detectors, mixers, and frequency multipliers. However, they are not able to handle high power due to its relatively low breakdown voltage and thermal conductivity. In this perspective, GaN is a promising material² since its wide bandgap allows it to manage much higher input power and can help to reduce the size and complexity (avoiding power-combining) of frequency multipliers.^{3–6} GaN SBDs may expand the practical application of THz technology to fields, such as security scanning, medical diagnosis, and ultrahigh-bandwidth wireless communications.⁷ For these applications, the high breakdown

voltage of GaN SBDs is a key parameter for increasing its power performance.⁸ However, its real breakdown voltage is effectively reduced from its ideal limit due to multiple mechanisms, typically related to traps and defects located in the epilayer or at the interface,⁹ such as Poole–Frenkel emission (PFE), tunneling assisted by traps (TAT), or variable range hopping, which generate an excess of current with respect to the one expected from the ideal mechanisms, thermionic emission, and direct tunneling current.^{10–13} In this work, we analyze in temperature nonideal reverse-leakage current mechanisms related to traps present in GaN SBDs fabricated on metalorganic chemical vapor deposition (MOCVD) grown layers on a sapphire substrate. A complete experimental characterization reaching temperatures down to 33 K, lower than those typically used in the literature, has allowed us to identify hysteretic behavior of the reverse current in dual-sweep measurements not previously described, which becomes notorious below 125 K. This effect is the main novelty of our work, which we explain in terms of some of the above leakage mechanisms.

25 November 2024 08:29:03

This paper is organized as follows. The structure of the measured diodes and the experimental setups are described in Sec. II. The results and their discussion are reported in Sec. III. Finally, the main conclusions are drawn in Sec. IV.

II. DEVICES AND EXPERIMENTAL SETUP

The diodes under analysis were fabricated on an epitaxial structure consisting of a 600 nm thick epilayer (with a doping of $5 \times 10^{16} \text{ cm}^{-3}$) and a 750 nm thick substrate of highly Si-doped GaN (10^{19} cm^{-3}) on a sapphire substrate. The Pt/Au Schottky contact is placed on the top of the epilayer, while the ohmic contact formed by Ti/Al/Ni/Au is on the highly doped GaN layer. The fabrication process is similar to that described in Ref. 14. Circular diodes with different sizes all along the wafer have been analyzed, finding similar effects. Despite devices are not passivated, in previous analysis (measuring circular diodes with diameters from $70 \mu\text{m}$ up to $1400 \mu\text{m}$), reverse-leakage current was found to be essentially proportional to the diode area indicating that edge effects are negligible.¹⁵ Here, we present results for a diode with a nominal diameter of $221 \mu\text{m}$; see Fig. 1.

Current-voltage (I - V) and capacitance-voltage (C - V) measurements have been performed at different temperatures, from 33 to 475 K, by means of a LakeShore CRX-VF cryogenic probe station. The experimental setup for the characterization of the diodes is different depending on the type of measurements. On one hand, the probe station is connected to an impedance analyzer

(Agilent E4980A) for the C - V measurements. On the other hand, the I - V curves were obtained using a semiconductor analyzer (Keithley 4200-SCS) and four continuously variable temperature probes (which allow temperature sweeps without the need to lift the needles, thus minimizing the damage of the pads). The semiconductor analyzer has three source measurement units (SMUs), which are used to perform the I - V measurements using the classic four-probe technique (two of them used as a current source and the other two to measure the real voltage difference between contacts).

III. RESULTS AND DISCUSSION

Firstly, C - V measurements were carried out from 100 kHz to 1 MHz for several temperatures (100, 200, 300, 400, and 475 K) and no frequency dependence was observed, indicating that bulk traps are not at the origin of the leakage-current mechanism. Figure 2 shows, as a function of temperature, the parameters extracted from the C - V - T analysis, performed at 1 MHz with $V_{osc} = 30 \text{ mV}$. The C^{-2} vs V characteristics, which exhibit the typical behavior of a SBD (linear with the applied voltage), is represented in the inset, allowing one to extract the epilayer doping, N_D (red); the built-in voltage, V_B (blue); and the barrier height, ϕ_B (pink), using the following equations:

$$C^{-2}(V) = \frac{2(V_B - V)}{S^2 q N_D \epsilon_{SC}}, \quad (1)$$

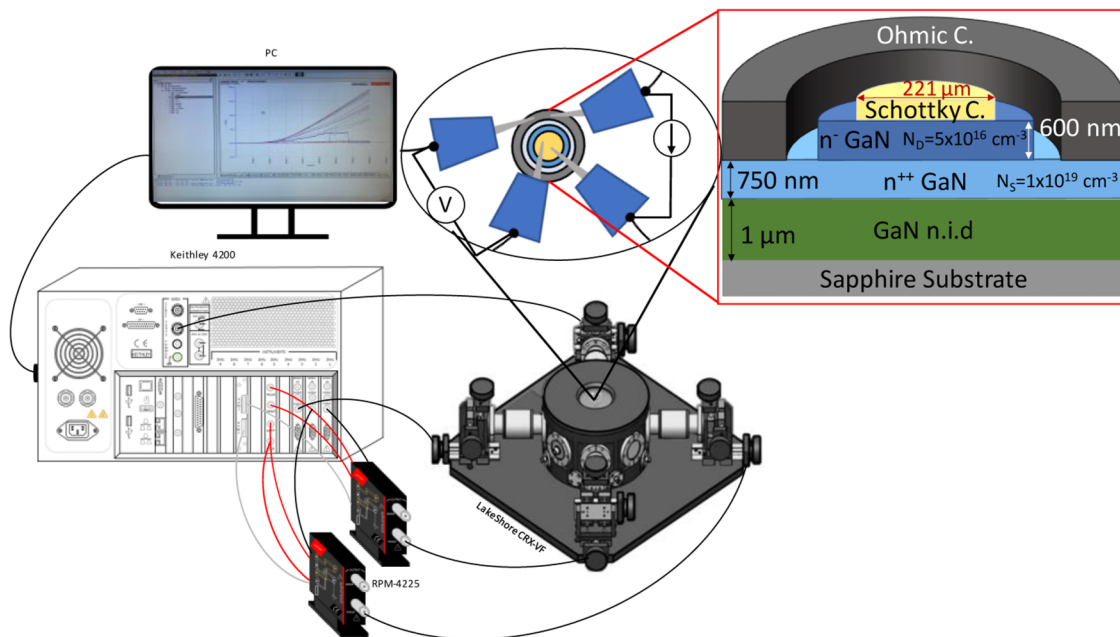


FIG. 1. Scheme of the experimental setup for measuring the I - V characteristics. A cryogenic probe station is used to carry out measurements in temperature. The probe station is connected to a semiconductor analyzer (Keithley 4200-SCS). Four probes are used to perform these measurements (two are used as a current source and the other two to measure the real voltage between terminals). A sketch of the SBD under analysis is also shown, where the position of the ohmic and Schottky contacts and the doping level and the thickness of the different layers are indicated.

$$\phi_B = V_B - \frac{k_B T}{q} \ln\left(\frac{N_D}{N_C}\right), \quad (2)$$

where S is the Schottky contact surface, q is the electron charge, ϵ_{SC} is the permittivity of the semiconductor, k_B is the Boltzmann constant, and N_C is the effective density of states in the conduction band.

Both ϕ_B and N_D remain practically constant with temperature, with values around 0.7–0.8 eV and $4.0\text{--}4.5 \times 10^{16} \text{ cm}^{-3}$, respectively. On the other hand, qV_B monotonously increases when decreasing T , from below 0.6 eV to around 0.75 eV, almost coinciding with ϕ_B for low T .

The I - V characteristic of the GaN SBD has been measured in dark conditions as a function of T . Figure 3 shows the dual-sweep J - V - T curves of the device (starting at 0 V) in (a) reverse and (b) forward bias, jointly with the results of the model developed in Ref. 14.

In forward bias, the model only includes the thermionic contribution, while in reverse bias, both thermionic (J_{th}) and direct tunneling currents (J_{tunnel}) are considered. The derivation of the expressions used to calculate these currents can be found in Ref. 14. A constant value for the doping of $4.5 \times 10^{16} \text{ cm}^{-3}$ has been used for all temperatures, as well as a series resistance of 1 Ω . The values of ϕ_B and η , shown in the inset of Fig. 3(b), have been extracted at each temperature by fitting the measurements in forward bias, ϕ_B then being used to predict the ideal contribution in reverse bias. Comparing the values of ϕ_B extracted from C - V and I - V curves, they are similar for the highest temperatures. However, for low T , ϕ_B obtained from the ideal current model shows a significant decrease (not observed in the value extracted from the capacitance) and η increases concurrently. This behavior, already found in the literature,^{16,17} is attributed to the presence of inhomogeneities of the barrier height.

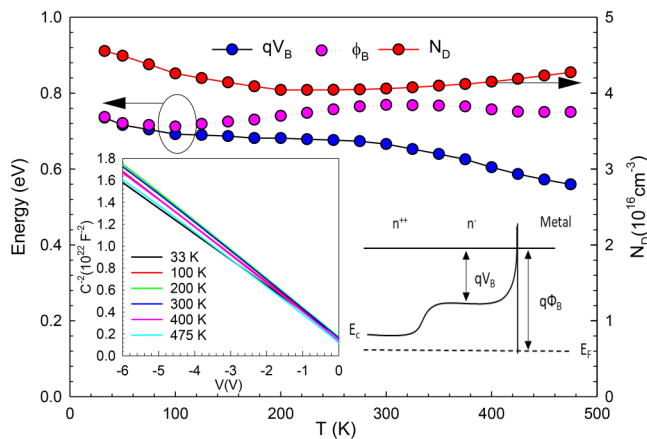


FIG. 2. Characteristic parameters of the SBD extracted from the C - V curves as a function of temperature. The left inset shows the linear behavior of the C^{-2} - V curve, revealing a slight variation with temperature. The conduction band diagram identifying the parameters V_B and ϕ_B is shown in the right inset.

Let us analyze now the reverse bias results. Figure 3(a) shows how the ideal model almost perfectly reproduces the behavior of the measurements, J_{exp} , for the highest temperatures. For temperatures from 400 to 225 K, the experimental curves start to deviate from the model in reverse bias, which evidences the progressive increase of the contribution of nonideal leakage mechanisms. For temperatures below 200 K, the results of the model are not represented in reverse bias since the values obtained are negligible with respect to the experimental ones. Interestingly, a hysteresis phenomenon not previously explored in detail for this kind of devices is found for the lower temperatures, whose origin will be explained later.

From these DC measurements, by comparison with the model, it is possible to extract the excess current density due to the non-ideal mechanisms as $J_{exc} = J_{exp} - J_{th} - J_{tunnel}$. This value is represented as a function of the inverse of temperature in Fig. 4(a). For the highest temperatures up to 400 K, J_{exc} is negligible as compared to the high values of J_{th} and J_{tunnel} and the reverse I - V curve of the SBD is nearly ideal. Thus, we calculate J_{exc} only for temperatures below 400 K. Two behaviors are observed: for high T , a temperature-dependent mechanism is present, while a temperature-independent one arises at low T . DC dual voltage sweep measurements for the reverse I - V curves were carried out by ramping up and down the negative voltage (see Fig. 4), overall taking about 200–300 s depending on the precision needed. In order to reset the trap occupancy, the devices are illuminated at the beginning of every dual-sweep measurement (the light source is the halogen bulb of the microscope, of 3250 K color temperature and 150 W power). Since a hysteresis cycle takes place, the current in excess has been represented for both directions of the sweep (go and return). While at high T , J_{exc} does not change between the go and the return, for low T , J_{exc} in the return sweep decreases with respect to the go sweep. Moreover, all the I - V curves tend to reach the same current at -30 V [see Fig. 3(a)].

Regarding the mechanism dominant at high temperatures, linear behavior with $1/T$ is observed in the return sweep of $\ln(J_{exc})$, indicating that it can be described as a PFE process, providing an excess current given by¹²

$$J_{PFE} \propto E \exp\left(\frac{-q(\phi_t - \sqrt{qE/\pi\epsilon_{sc}})}{k_B T}\right), \quad (3)$$

where E is the maximum electric field (that appears at the metal–semiconductor interface)¹⁸ and ϕ_t is the energy level of the trap at the origin of the PFE process. The permittivity of the GaN used in this work is $8.9\epsilon_0$,¹⁹ being ϵ_0 the vacuum permittivity. PFE consists of the thermal promotion of an electron from a trap into the conduction band, process which is fed by tunneling from the metal in reverse bias conditions. Following Eq. (3), the fitting of $\ln(J_{exc})$ vs $1/T$, as shown in Fig. 4(b), allows one to obtain the energy level of the trap producing the PFE mechanism, which is around 0.2 eV.

On the other hand, for low T , J_{exc} is nearly constant with temperature, as observed in Fig. 4(a). Such behavior is typically due to

25 November 2024, 08:29:03

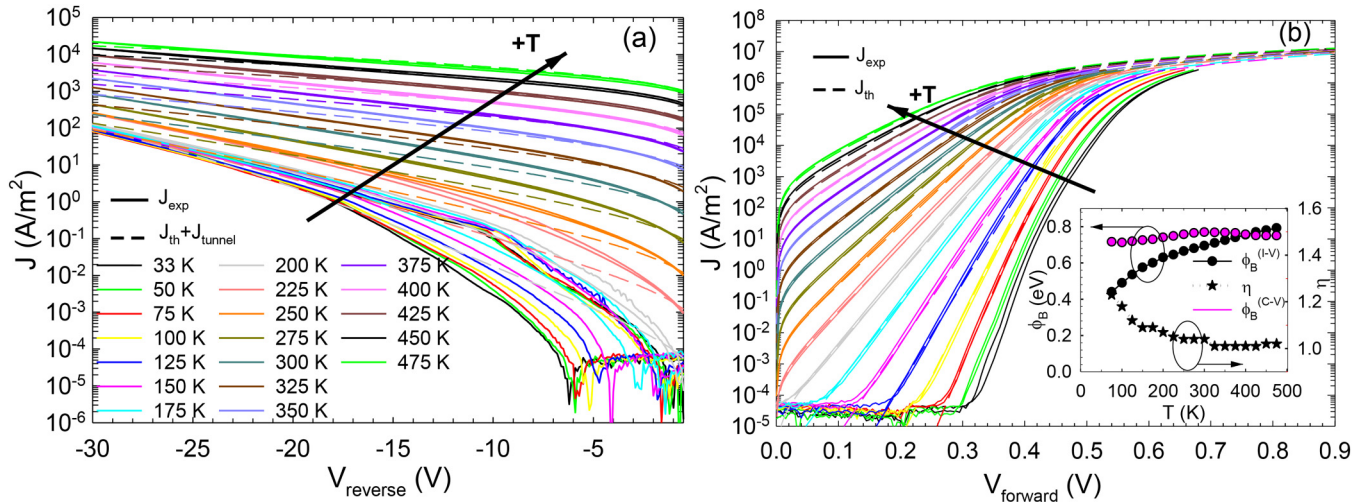


FIG. 3. J - V curves measured (solid lines) and modeled (dashed lines) for (a) reverse and (b) forward bias. The inset includes ϕ_B and extracted from the fitting of the ideal model and the experimental curves in forward bias (in black), as well as ϕ_B extracted from the C - V curves (in pink).

TAT, whose associated leakage current is given by¹²

$$J_{TAT} \propto \exp\left(\frac{-4\sqrt{2qm^*}\phi_t^{3/2}}{3\hbar E}\right), \quad (4)$$

where \hbar is the Planck constant and m^* is the effective mass of the electrons (in our case $0.22m_0$).²⁰ The representation of $\ln(J_{exp})$ at low T (100 K) in the go and return sweeps as a function of the inverse of the maximum electric field is provided in Fig. 4(c). At other (low) values of temperature, similar behavior is found. The observed linear dependence in different ranges of $1/E$ indicates the presence of TAT mechanisms. TAT allows the tunnel injection of electrons from the metal to the semiconductor through the trap states as long as these are not occupied.

In Fig. 4(c), two slopes, corresponding to different traps, can be distinguished. The energy level extracted for these trap states is around 0.2 eV for trap 1 and around 0.45 eV for trap 2. Interestingly, the energy of trap 1 is very similar to that at the origin of PFE at higher temperatures, which means that as electrons do not have the enough thermal energy to be injected by PFE, they use the same trap to tunnel into the semiconductor. Since the lack of frequency dispersion in C - V measurements allows one to discard bulk traps as the cause of the observed hysteresis, we attribute it to interfacial defects. Note that this kind of surface states with similar energy levels has been found in other works analyzing leakage current in GaN SBDs.⁹

The go curve in Fig. 4(c) exhibits a higher current level with respect to the return one. For low values of reverse bias (low electric field, linear dependence on $1/E$), the current due to electrons tunneling through trap 1 is dominant because the trap states are located closer to the conduction band. When the reverse applied voltage is increased, the influence of trap 2 starts being significant

due to the narrowing of the barrier so that the probability of electrons tunneling through trap 2 increases, as well as the slope of the curve. A transition between TAT processes dominated by each of the traps takes place around a value of $1/E$ of 2.7 cm/MV. If the applied voltage is further increased, some of the trap states become occupied and the current increase is softer. When decreasing the reverse applied voltage, a lower current level is measured in the return curve. For the highest voltages (highest electric fields), linear behavior of $\ln(J_{exc})$ with respect to $1/E$ is found again, which fits the TAT dependence described by Eq. (4) with the energy of trap 2.

The explanation to this behavior is as follows. As the applied voltage is raised in the go sweep, the occupancy of both traps increases, first that of the lower-energy trap 1 and then that of trap 2 for the highest voltages. When the bias is decreased in the return sweep, due to the fact that some of the trap states remain occupied, mainly those of trap 1, TAT processes are less frequent and obviously, the current is lower than in the go sweep. Even if both traps have a higher occupancy, the effect of trap 1 on the current is more significant due to its closer proximity to the conduction band as compared with trap 2. Thus, while the lower concentration of free traps has an important effect on the current for the case of trap 1, by drastically reducing the associated TAT processes, in the case of trap 2, it is not so crucial, and it is this trap that dominates the TAT current in the return sweep.²¹ Also, the capture cross section of the traps could be important.

If few seconds after a first dual voltage sweep measurement a second one is performed without illumination in between, both the go and return curves essentially coincide with the return curve of the initial sweep, indicating that the traps remain occupied. The initial hysteresis cycle is recovered only if trapped electrons are released, either by illuminating the sample (during some seconds) or waiting for their thermal emission (taking several days). Additionally, pulsed measurements applying different base voltages

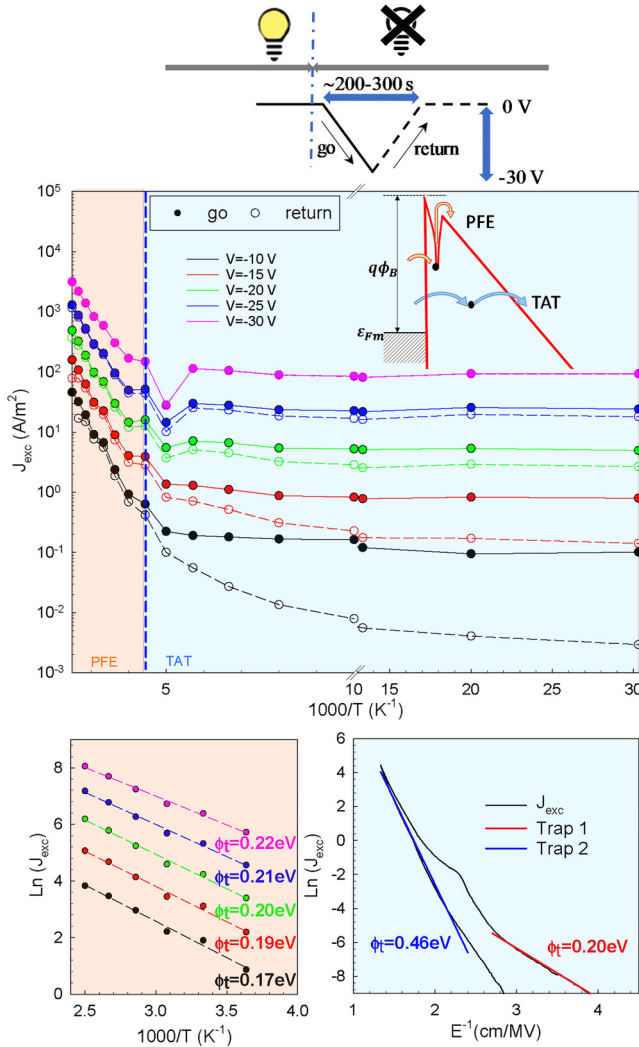


FIG. 4. (a) Excess of reverse current as a function of $1/T$ (from 33 to 400 K) for different bias points. The inset shows the schematic representation of the non-ideal current mechanisms, PFE and TAT. Fitting of the results to the characteristic dependence of the (b) Poole-Frenkel emission for the highest temperatures and (c) trap-assisted tunneling at low temperatures (100 K in this case). On the top, the time dependence of the applied voltage in dual-sweep measurements is shown.

(of 0, -20 , and -30 V) prior to each measured point were performed, evidencing higher initial occupancy of the trap states linked to higher base voltages. All these facts confirm that the hysteresis observed in the reverse I - V curves is due to electron trapping impeding the current flow through TAT processes. This effect has been found in all the diodes of the wafer, with just a little variability in the voltage range and the current levels for which the hysteresis takes place, but with the same qualitative behavior. The trap energies obtained are in a narrow range of 0.18 – 0.22 eV and 0.46 – 0.50 eV, respectively.

IV. CONCLUSIONS

In summary, the reverse current of GaN on sapphire SBD has been analyzed from 33 to 475 K. While it shows nearly ideal behavior for the highest temperatures, below 400 K, an extra leakage-current contribution with respect to the ideal one is obtained. The analysis of this current in excess has clearly evidenced the presence of two mechanisms related to traps. For temperatures above 200 K, PFE through a trap with an energy level around 0.2 eV is dominant, while for lower temperatures, TAT is the prevailing mechanism. Remarkably, two different traps contribute to the TAT current, causing a hysteresis phenomenon in the reverse I - V curves. The energies of these traps are around 0.2 eV (trap 1, the same one that provokes PFE) and 0.5 eV (trap 2). The hysteresis is caused by the increase in the occupancy of both trap states as the reverse bias is raised and the stronger influence of the occupancy of trap 1 on the current level.

ACKNOWLEDGMENTS

This work has been partially supported through Grant No. PID2020-115842RB-I00 funded by MCIN/AEI/10.13039/501100011033, Grant No. SA136P23 by the Junta de Castilla y León and FEDER, and by the French project SchoGaN (No. ANR-17-CE24-0034). R. A. Peña acknowledges the “Investigo” contract funded by the Junta de Castilla y León and by “European Union NextGenerationEU/PRTR.”

AUTHOR DECLARATIONS

Conflict of Interest

The authors have no conflicts to disclose.

Author Contributions

B. Orfao: Conceptualization (equal); Data curation (equal); Formal analysis (equal); Investigation (equal); Methodology (equal); Software (equal); Writing – original draft (equal); Writing – review & editing (equal). **M. Abou Daher:** Investigation (supporting); Methodology (equal); Resources (lead); Writing – review & editing (equal). **R. A. Peña:** Conceptualization (supporting); Formal analysis (supporting); Investigation (supporting); Methodology (equal); Writing – review & editing (equal). **B. G. Vassallo:** Conceptualization (supporting); Formal analysis (supporting); Investigation (supporting); Methodology (equal); Software (equal); Writing – review & editing (equal). **S. Pérez:** Conceptualization (supporting); Formal analysis (supporting); Investigation (supporting); Methodology (equal); Software (equal); Writing – review & editing (equal). **I. Íñiguez-de-la-Torre:** Investigation (supporting); Methodology (equal); Resources (equal); Writing – review & editing (equal). **G. Paz-Martínez:** Investigation (supporting); Methodology (equal); Resources (equal); Writing – review & editing (equal). **J. Mateos:** Conceptualization (equal); Data curation (equal); Formal analysis (equal); Investigation (equal); Methodology (equal); Software (equal); Supervision (lead); Writing – review & editing (lead). **Y. Roelens:** Investigation (supporting); Methodology (equal); Resources (lead); Writing – review & editing (equal). **M. Zaknune:** Investigation (supporting); Methodology

(equal); Resources (lead); Writing – review & editing (equal).
T. González: Conceptualization (equal); Data curation (equal);
Formal analysis (equal); Investigation (equal); Methodology (equal);
Software (lead); Supervision (lead); Writing – review & editing (lead).

DATA AVAILABILITY

The data that support the findings of this study are available from the corresponding author upon reasonable request.

REFERENCES

- ¹H. Eisele, *Electron. Lett.* **46**, S8–S11 (2010).
- ²J. M. Schellenberg, *IEEE Trans. Microw. Theory Tech.* **63**, 2833–2840 (2015).
- ³Y. Zhang, M. Sun, D. Piedra, M. Azize, X. Zhang, T. Fujishima, and T. Palacios, *IEEE Electron Device Lett.* **35**, 618–620 (2014).
- ⁴Z. H. Feng, S. X. Liang, D. Xing, J. L. Wang, D. B. Yang, Y. L. Fang, L. S. Zhang, and X. Y. Zhao, in *2016 IEEE MTT-S International Microwave Workshop Series on Advanced Materials and Processes for RF and THz Applications (IMWS-AMP)* (IEEE, 2016), pp. 1–3.
- ⁵B. Zhang, D. Ji, D. Fang, S. Liang, Y. Fan, and X. Chen, *IEEE Electron Device Lett.* **40**, 780–783 (2019).
- ⁶S. Liang, X. Song, L. Zhang, Y. Lv, Y. Wang, B. Wei, Y. Guo, G. Gu, B. Wang, S. Cai, and Z. Feng, *IEEE Electron Device Lett.* **41**, 669–672 (2020).
- ⁷D. Mittleman, *Sensing with Terahertz Radiation* (Springer, 2013), Vol. 85.
- ⁸X. Guo, Y. Zhong, X. Chen, Y. Zhou, S. Su, S. Yan, J. Liu, X. Sun, Q. Sun, and H. Yang, *Appl. Phys. Lett.* **118**, 243501 (2021).
- ⁹T. Hashizume, J. Kotani, and H. Hasegawa, *Appl. Phys. Lett.* **84**, 4884 (2004).
- ¹⁰E. J. Miller, E. T. Yu, P. Waltereit, and J. S. Speck, *Appl. Phys. Lett.* **84**, 535 (2004).
- ¹¹P. Pipinys and V. Lapeika, *J. Appl. Phys.* **99**, 093709 (2006).
- ¹²K. Fu, H. Fu, X. Huang, T. H. Yang, C. Y. Cheng, P. R. Peri, H. Chen, J. Montes, C. Yang, J. Zhou, X. Deng, X. Qi, D. J. Smith, S. M. Goodnick, and Y. Zhao, *IEEE J. Electron Devices Soc.* **8**, 74–83 (2020).
- ¹³J. Chen, Z. Liu, H. Wang, X. Song, Z. Bian, X. Duan, S. Zhao, J. Ning, J. Zhang, and Y. Hao, *Appl. Phys. Express* **14**, 104002 (2021).
- ¹⁴B. Orfao, G. D. Gioia, B. G. Vasallo, S. Perez, J. Mateos, Y. Roelens, E. Frayssinet, Y. Cordier, M. Zaknونة, and T. Gonzalez, *J. Appl. Phys.* **132**, 044502 (2022).
- ¹⁵G. Di Gioia, V. K. Chinni, M. Zegaoui, Y. Cordier, A. Maestrini, J. Treuttel, G. Ducourneau, Y. Roelens, and M. Zaknونة, in *Proceedings of 43rd Workshop on Compound Semiconductor Devices and Integrated Circuits (WOCSDICE), Cabourg, France, June 2019* (hal-03384353) (MDPI, 2019).
- ¹⁶K. Ejderha, S. Duman, C. Nuhoglu, F. Urhan, and A. Turut, *J. Appl. Phys.* **116**, 234503 (2014).
- ¹⁷M. Gülnahar, *Superlattices Microstruct.* **76**, 394–412 (2014).
- ¹⁸P. K. Rao, B. Park, S. T. Lee, Y. K. Noh, M. D. Kim, and J. E. Oh, *J. Appl. Phys.* **110**, 013716 (2011).
- ¹⁹O. Madelung, *Semiconductors: Data Handbook* (Springer, Berlin, 2004).
- ²⁰S. García, S. Pérez, I. Íñiguez-De-La-Torre, J. Mateos, and T. González, *J. Appl. Phys.* **115**, 044510 (2014).
- ²¹W. K. Loke, S. F. Yoon, S. Wicaksono, K. H. Tan, and K. L. Lew, *J. Appl. Phys.* **102**, 054501 (2007).